Applied Catalysis A: General 362 (2009) 8–13

Contents lists available at ScienceDirect

Applied Catalysis A: General

journal homepage: www.elsevier.com/locate/apcata

Interactions of SO_2 and H_2S with amorphous carbon films

W. Michalak [a,b], E. Broitman [b], M.A. Alvin [a], A.J. Gellman [a,b], J.B. Miller [a,b,*]

[a] National Energy Technology Laboratory, U.S. Department of Energy, Pittsburgh, PA 15236-0940, United States
[b] Department of Chemical Engineering, Carnegie Mellon University, Pittsburgh, PA 15213-3890, United States

ARTICLE INFO

Article history:
Received 9 February 2009
Received in revised form 2 April 2009
Accepted 4 April 2009
Available online 11 April 2009

Keywords:
Activated carbon
Hydrogen sulfide
Sulfur dioxide
Sulfur adsorption
Thin carbon films

ABSTRACT

There is significant interest in development of efficient catalyst-sorbents for the capture and conversion of sulfur-compounds such as H_2S and SO_2. In this work, ultra-high vacuum (UHV) techniques have been used to carefully prepare and thoroughly characterize amorphous carbon (a-C) thin films as models of activated carbon sorbents. Films with modified surface chemistries were prepared by oxidation of a sputter deposited carbon film (a-CO_x) and by sputter depositing carbon in the presence of N_2 (a-CN_x) or methane (a-CH_x). Temperature programmed desorption (TPD) and X-ray photoelectron spectroscopy (XPS) were used to study H_2S and SO_2 surface chemistry on these films and on a highly oriented pyrolytic graphite (HOPG) reference-surface. The modification of the carbons with different heteroatoms influences both the strength of their interactions with SO_2 and H_2S and their capacities for sulfur-compound adsorption.

1. Introduction

Sulfur-compounds, including hydrogen sulfide (H_2S) and sulfur dioxide (SO_2), frequently appear as contaminants in process streams in the production, processing and refining of fossil fuels [1–4]. Emissions of these compounds are regulated because of their potential for adverse health and environmental effects. H_2S poisons water-gas-shift catalysts and hydrogen separation membranes used in integrated gasification combined cycle (IGCC) processes for electricity production from coal. Many current-generation technologies for removal of sulfur-compounds from gas streams are based on absorption by liquids, usually amine solutions or oxygenated solvents. Amine-based systems are suitable for current emissions requirements, but cannot achieve future regulation levels; processes based on oxygenated solvents are typically expensive and energy intensive [5,6].

Solid sorbents have seen growing interest for both capture and conversion of sulfur-compounds. Low-cost, environmentally benign activated carbon is unique among solid sorbents because of its high surface area (as high as 3000 m^2/g), its pore size distribution (typically in the 5–30 Å range), its broad range of surface functional groups, and its relatively high mechanical strength [1,7–9]. Activated carbon can be used at typical flue gas outlet temperatures, so there is no need to cool or reheat the process stream. Both chemical interactions, which depend on the chemical nature of the adsorbate, co-adsorbates and the surface, and physical factors, which include size exclusion and pore-diffusion, influence the capture of molecules by activated carbons [9,10]. Carbons can also promote partial catalytic oxidation reactions, providing the potential for conversion of the captured sulfur-compounds to valuable commodity chemicals [3–6,11].

Generally, carbon surfaces are non-polar and, thus, will not adsorb polar molecules. Activation of the carbon increases its affinity for adsorption of polar species such as H_2S and SO_2. Activated carbon is derived from materials with high carbon contents such as coal, wood, lignite, and peat [9]. The activation process consists of two primary steps: pulverization and exposure to high temperatures [5,9]. The process forms an amorphous heterogeneous carbon matrix in a random ordering of imperfect aromatic ("graphene") sheets [12]. Within the carbon sheets, two carbon atom hybridizations, sp^2 and sp^3, typically exist in an 80:20 ratio [13,14]. As shown schematically in Fig. 1a, most carbon atoms in the sheet are organized in high atom-density basal planes with 3-fold sp^2 coordination, forming σ-bonds in hexagonal rings [15]. These planes form parallel layers, as in graphite, so that the fourth valence electron of the sp^2 atom lies in a π-orbital normal to the σ-bonding plane. Surface defects, which are often active for chemisorption, most frequently appear at the edges of misaligned graphene sheets. They can have the form of sp^2-hybridized carbon atoms with incompletely saturated valences or sp^3-hybridized carbon atoms with both unpaired electrons and unsaturated valences [9,12–14]. Activation also significantly reduces the number of organic compounds adsorbed on the carbon surface,

* Corresponding author.
E-mail address: jbmiller@andrew.cmu.edu (J.B. Miller).

0926-860X/$ – see front matter © 2009 Elsevier B.V. All rights reserved.
doi:10.1016/j.apcata.2009.04.008

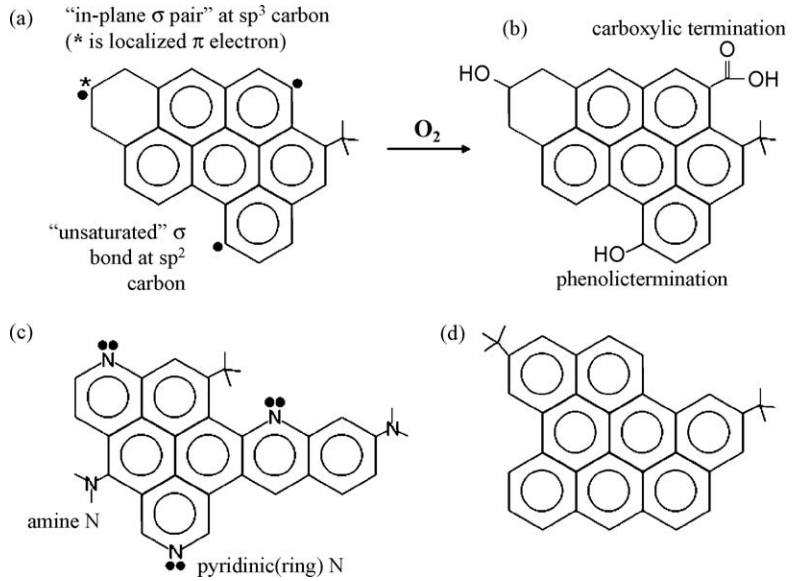

Fig. 1. Models of basal plane sheets and surface defects of carbon surfaces, (adapted from [15]). (a) a-C, with unsaturated sigma bond (sp^2) and in-plane sigma pair (sp^3) edge defects, (b) a-CO_x, with edge defects capped by formation of carboxylic or phenolic groups, (c) c-CN_x, with no (few) edge defects, (d) a-CH_x (similar to HOPG), with no (few) edge defects.

while heteroatoms such as oxygen, nitrogen, and hydrogen all remain to differing degrees [10].

Previous studies of activated carbon as a catalytic sorbent for sulfur-compounds have focused on behavior under dynamic conditions at atmospheric pressure and report material performance in breakthrough capacity tests. These studies have addressed the effects of gas composition, temperature, pressure, microporosity, heteroatoms/surface modifiers, metal dopants, the acidic/basic nature of the surface, the role of solvents, most notably water, and the possibilities for thermal regeneration [1,3,4,7,8,10,16–22]. However, little is known at the molecular level about the nature of sulfur-compound adsorption onto carbonaceous surfaces. In this work, we prepare a set of well-controlled model carbon surfaces and apply the methods of ultra-high vacuum (UHV) surface science to determine how microstructure and surface chemical modification influence adsorption capacity and desorption kinetics for H_2S and SO_2. This approach allows us to isolate and understand important elementary steps in capture of sulfur-compounds by carbon surfaces; our results will contribute to a basis for rational design of next-generation activated carbons for fossil fuel application.

2. Experimental details

All experiments were carried out in a stainless steel UHV chamber evacuated with a turbomolecular pump, a cryogenic pump, and a titanium sublimation pump to a base pressure of 10^{-9} Torr. The chamber is equipped with an X-ray photoelectron spectrometer (XPS) system for verification of the cleanliness of deposition substrates and surface chemistry of the films. XPS measurements were carried out with a single pass hemispherical energy analyzer and an X-ray source operating at 13 kV and 20 mA at an angle of incidence of 54.7° to the sample. Additional details of the apparatus have been described elsewhere [23].

A homogeneous HOPG (highly oriented pyrolytic graphite, 12 mm × 12 mm × 2 mm) substrate was used as a reference carbon surface in this work. The HOPG crystal was mounted in a Ni foil sample holder. To improve thermal contact, Ag paste was applied between the HOPG crystal and the holder. Carbon thin films were deposited onto a polycrystalline Ni substrate (12.5 mm diameter × 0.5 mm) using a DC magnetron sputtering source. Both the Ni foil and the Ni substrate were mounted, via Ta leads, to a copper block which was cooled with liquid nitrogen to 90 K and resistively heated to 1000 K. The temperature was measured with a chromel-alumel (K-type) thermocouple spot welded to the back side of the Ni.

The HOPG surface was cleaned outside of the chamber by cleaving the top layer with Scotch™ tape to remove the topmost crystalline layers and to expose a new basal plane. In UHV the HOPG was annealed to 1000 K. The Ni substrate was cleaned outside of the chamber by polishing with Buehler MetaDi® II 1 μm diamond polish. Further cleaning was performed in vacuum by cycles of Ar^+ sputtering followed by 1000 K anneals to remove the primary contaminant (oxygen) to less than ~3 at.% (determined by XPS) before carbon film deposition.

Four types of sputtered carbon thin films were prepared: amorphous carbon (a-C), oxidized amorphous carbon (a-CO_x), amorphous carbon nitride (a-CN_x), and amorphous hydrogenated carbon (a-CH_x). All films were deposited with 75 W power, using a 1.3″ high-purity (99.99%) pyrolytic graphite target. Gases used for thin film deposition were introduced via mass flow controllers. The a-C surface was prepared in an Ar plasma at a pressure of 8 mTorr [24]. During the 15 min deposition, the nickel substrate was held at 600 K, with a floating bias [24]. The a-CO_x film was initially prepared in the same manner as the a-C film, but was subsequently exposed to O_2 at a pressure of 6×10^{-4} Torr for approximately 10 h [24,25]. X-ray photoemission analysis of the product film revealed a surface concentration of atomic oxygen ranging from 10 to 15 at.%, similar to oxygen contents reported for commercial activated carbons [16,17]. The a-CN_x film was prepared in an atmosphere of N_2 at a pressure of 5 mTorr [24,26]. The unbiased sample was heated to a temperature of 500 K during the 20 min deposition [24,26]. The a-CH_x film was prepared in a 7:1 Ar:CH_4 gas mixture at a pressure of 8 mTorr. The electrically grounded sample was heated to a temperature of 443 K during the 25 min deposition [26].

The nature of the interactions between the sulfur-compounds and the carbon surfaces was characterized in temperature programmed desorption (TPD) experiments. TPD provides insight into desorption kinetics and allows estimation of the energy of desorption, E_{des}, a measure of the strength of the affinity that the surface has for the adsorbed molecule. For the TPD experiments,

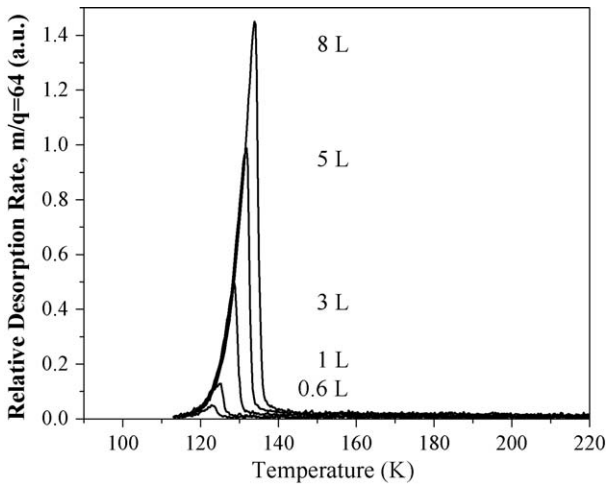

Fig. 2. Temperature programmed desorption of SO_2 from the HOPG surface for a series of different exposures. Exposures were performed with the HOPG at 100–110 K; the heating rate was 0.5 K/s. Peak shapes are characteristic of zero-order desorption kinetics.

the carbon surfaces were exposed to H_2S or SO_2 (Matheson Tri Gas, research grade) introduced into the chamber via an external leak valve. A quadrupole mass spectrometer (QMS) was used as a detector for the desorbing molecules. TPD of SO_2 and H_2S from HOPG was performed by first exposing the surface to adsorbate at 100–110 K and then monitoring SO_2 (m/q = 64) or H_2S (m/q = 34) desorption with the QMS while heating the surface at 0.5 K/sec. TPD from the sputter-deposited amorphous carbon surfaces was performed by exposing the surface to SO_2 or H_2S at temperatures between 89 and 92 K and then monitoring desorption of the species with the QMS while heating the surface at 1 K/s.

3. Results and discussion

3.1. TPD of SO_2 from the carbon surfaces

Fig. 2 displays the thermal desorption spectra of SO_2 from the HOPG surface for exposures from 0.6 to 8 L (1 L = 10^{-6} Torr s). The shapes of the TPD spectra-common leading edges followed by rapid fall to zero desorption rate upon depletion of adsorbed molecules – are characteristic of zero-order desorption kinetics [27]. Using the leading edge analysis of Habenschaden and Kuppers [28], E_{des}, the energy of desorption for SO_2 from HOPG was estimated to be 35 ± 1 kJ/mol. This value is consistent with E_{des} for SO_2 desorption from multilayers on other surfaces [29,30] and is only slightly higher than SO_2's heat of sublimation, ΔH_{sub} = 32.32 kJ/mol [31]. These results suggest a cooperative adsorption mechanism in which adsorbate–adsorbate attractive interactions play a significant role, resulting in condensation of the polar SO_2 molecules on the surface as multilayer islands or clusters [32]. The condensed molecules are bound to the surface via weak van der Waals interactions with the π-electrons in the aromatic rings of the carbon surface [9].

The TPD spectra of SO_2 from the a-C surface following adsorption using exposures between 0.3 and 13 L are shown in Fig. 3. The peak shapes are very different from those observed for desorption from the HOPG surface. They display a distinct asymmetry, with peak temperatures that decrease with increasing exposure. This behavior is similar to that observed for desorption of alcohols and ethers from amorphous carbon surfaces. The decrease in the peak desorption temperature with increasing coverage is usually associated with second-order (bimolecular) desorption kinetics, but it is not likely that molecular desorption of SO_2 occurs via a second-order process. The decrease in the peak desorption temperature could also arise from repulsive interactions between adsorbed SO_2 molecules resulting in a differential heat of adsorption that decreases with coverage. This also seems unlikely, given that desorption of SO_2 from the HOPG surface displays zero-order desorption kinetics (Fig. 2), suggesting that SO_2 molecules condense rather than repel one another.

A more likely scenario is that SO_2 desorbs with first-order kinetics from an energetically heterogeneous a-C surface. On the energetically heterogeneous surface, mobile adsorbed molecules sample available adsorption sites and choose those with the highest affinity for binding [9]. As the surface continues to fill at increasing coverages, adsorbed molecules must choose sites with lower binding energies. Peak temperatures for SO_2 desorption from a-C vary from 175 K at the lowest exposure to 145 K at the highest exposure. Based on a first-order Redhead analysis with a pre-exponential factor of $\nu = 10^{13}$ s^{-1} [33], these peak temperatures correspond to desorption energies, E_{des}, that decrease from 47 ± 1 (lowest exposure) to 36 ± 1 kJ/mole (highest exposure). The observations of first-order rather than zero-order desorption kinetics and higher values of E_{des} illustrate that the a-C surface has a stronger affinity for SO_2 than does HOPG. This difference probably reflects the contribution of defects at the periphery of graphene sheets on the a-C surface, as illustrated in Fig. 1a. The observation of an energetically heterogeneous surface is consistent with the presence of more than one type of edge site.

Fig. 4 displays the thermal desorption spectra of SO_2 from the a-CO_x surface for exposures between 0.5 and 20 L. As was the case for a-C, SO_2 desorbs from a-CO_x with first-order kinetics and values of E_{des} that decrease with increasing coverage. The values of E_{des} for SO_2 on the a-CO_x surface vary from 46 ± 1 (lowest exposure) to 38 ± 1 (highest exposure). This E_{des} range is the same as was observed for first-order desorption of SO_2 from a-C, suggesting that the *strength* of interaction between SO_2 and these two surfaces is similar. Fig. 5 shows the relative amounts of SO_2 that desorb from a-C and a-CO_x as a function of exposure. At all exposures, a-C desorbs almost twice as much SO_2 as does a-CO_x. Assuming similar sticking coefficients for SO_2 adsorption onto a-C and a-CO_x, oxygen treatment appears to reduce the *density* of sites for SO_2 adsorption, perhaps by capping defect sites at the edges of the graphene sheets as phenolic or carboxylic groups, as illustrated in Fig. 1b.

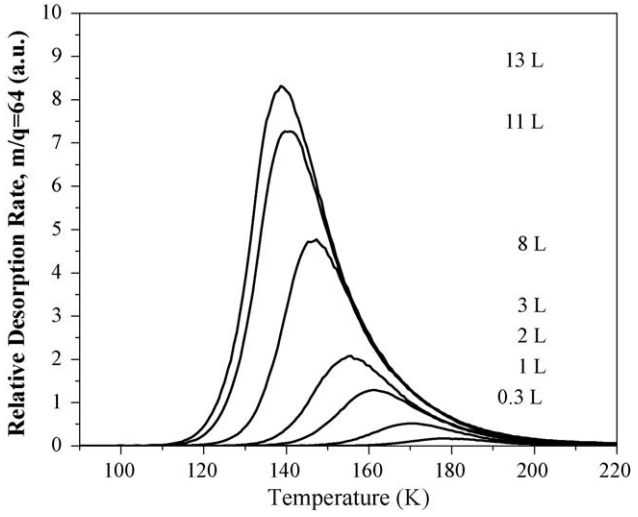

Fig. 3. Temperature programmed desorption of SO_2 from the a-C surface for a series of different exposures. Exposures were performed at ~90 K; the heating rate was 1 K/s. Peak shapes suggest first-order desorption from an energetically heterogeneous surface.

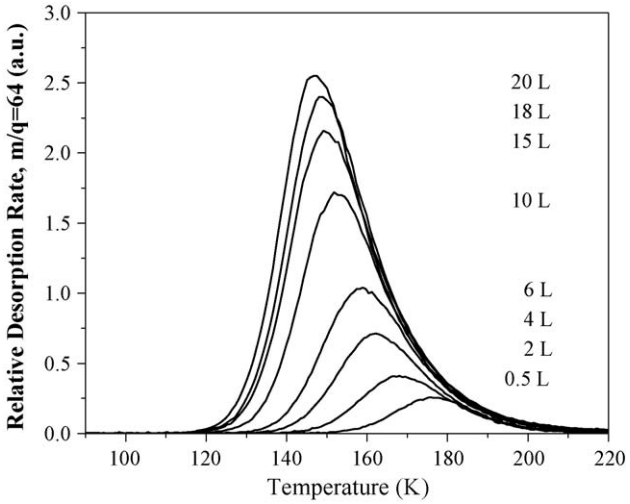

Fig. 4. Temperature programmed desorption of SO_2 from the a-CO_x surface for a series of different exposures. Exposures were performed at ~90 K. The heating rate was 1 K/s. Peak shapes suggest first-order desorption from an energetically heterogeneous surface.

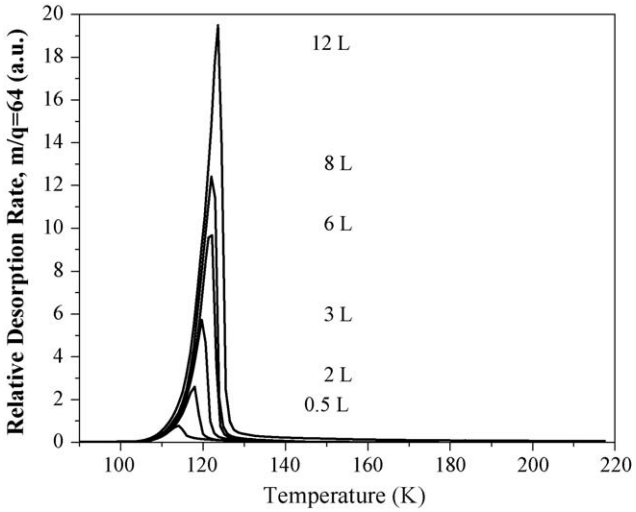

Fig. 6. Temperature programmed desorption of SO_2 from the a-CN_x surface for a series of different exposures. Exposures were performed at ~90 K; the heating rate was 1 K/s. Peak shapes are characteristic of zero-order desorption kinetics.

TPD spectra of SO_2 from the a-CN_x surface for exposures between 0.5 and 12 L appear in Fig. 6. As was observed for HOPG, peak shapes are consistent with zero-order desorption kinetics. E_{des} for SO_2 desorption from a-CN_x, estimated by leading edge analysis, is 33 ± 1 kJ/mol. This value is marginally lower than E_{des} estimated for SO_2 desorption from HOPG, suggesting that the SO_2 interaction with the a-CN_x aromatic π-system may be slightly weaker than in HOPG. Fig. 7 displays the N1s XPS spectrum of the a-CN_x film. The spectrum can be deconvoluted as two features at 400.8 eV (P1, FWHM = 2.7 eV) and 398.6 eV (P2, FWHM = 2.1 eV). The feature at 400.8 eV can be assigned to 3-fold coordinated nitrogen in a sp^2 carbon environment, i.e. substitutional graphite sites [26]. While its origin is less certain, Hellgren et al. suggest that the feature at 398.6 eV corresponds to either 3-fold coordinated nitrogen in a sp^3-hybridized carbon matrix or in a pyridine-like structure where 2-fold coordinated sp^2-hybridized nitrogen forms two bonds at the edge of the graphitic structure [26]. A model of the a-CN_x surface which is consistent with these observations appears in Fig. 1c. Without the unsaturated edge defect sites that characterize a-C, a-CN_x bears a strong resemblance to HOPG and the mechanisms for interaction between SO_2 and the surface are likely similar in the two cases. However, the presence of N-atoms may cause some subtle differences. For example, ring-N can withdraw electron density from the π-sites, thus decreasing the strength of the dispersion forces [12]. This effect could be responsible for the slightly lower E_{des} (relative to HOPG) observed for a-CN_x. Significantly, the basic surface groups in a-CN_x do not appear to generate new surface adsorption sites.

The TPD spectra of SO_2 from the a-CH_x surface for exposures between 0.5 and 12 L, shown in Fig. 8, display the characteristic zero-order peak shape. E_{des}, estimated by analysis of the leading edges, is 32 ± 1 kJ/mol. This value is slightly lower than E_{des} of SO_2 from HOPG and equivalent to E_{des} of SO_2 from a-CN_x; it is comparable to ΔH_{sub} of SO_2. The mechanism for adsorption is likely the same as described earlier for SO_2 on both HOPG and a-CN_x. During growth of the a-CH_x film, the surface defects associated with higher values of E_{des} and first-order desorption kinetics either do not form or are reduced by hydrogen atoms, creating a surface that is much like HOPG (Fig. 1d), with only π-electrons available for weak interaction with SO_2. The slightly lower value of E_{des} observed for the a-CH_x surface may reflect a smaller aromatic domain than in HOPG.

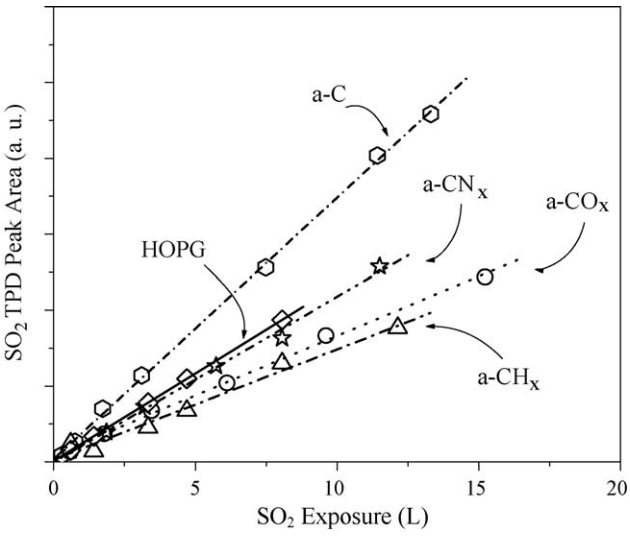

Fig. 5. Relative quantities of SO_2 desorbed (measured as thermal desorption peak area) as a function of exposure for the five carbon surfaces.

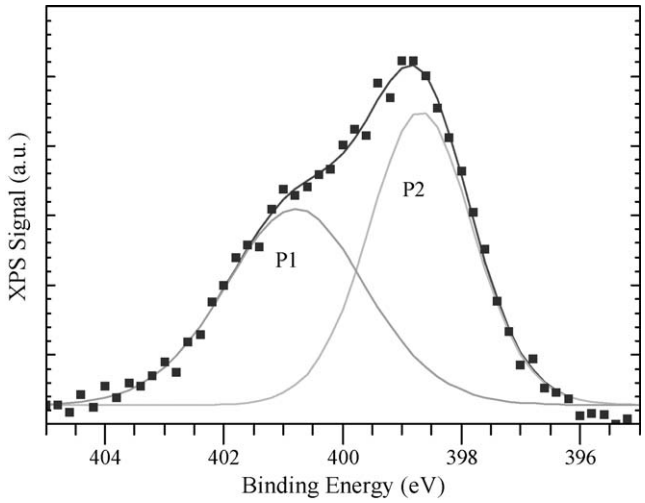

Fig. 7. N 1s region of the XPS spectrum of a-CN_x film. P1 corresponds to substitutional graphite sites. P2 corresponds to either N in a 3-fold coordinated sp^3-hybridized carbon state or in a pyridine-like structure at the edge of the graphene sheets.

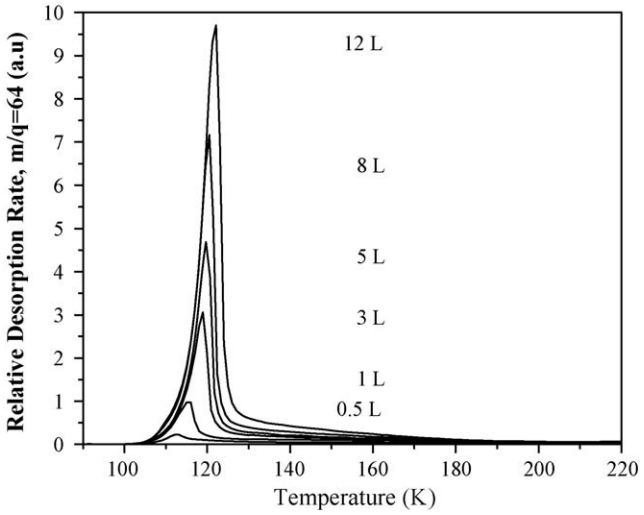

Fig. 8. Temperature programmed desorption of SO_2 from the a-CH_x surface for a series of different exposures. Exposures were performed at ~90 K; the heating rate was 1 K/s. Peak shapes are characteristic of zero-order desorption kinetics.

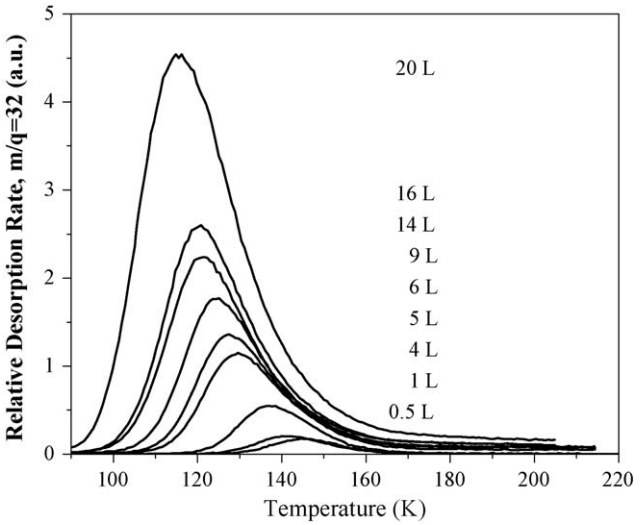

Fig. 10. Temperature programmed desorption of H_2S from a-CO_x for different exposures. Exposures were performed at ~90 K; the heating rate was 1 K/s. Peak shapes suggest first-order desorption from an energetically heterogeneous surface.

As noted during the discussion of SO_2 adsorption on a-CO_x, different surfaces can display different capacities for SO_2 adsorption. Fig. 5 includes plots of the TPD peak area as a function of exposure for each of the carbon surfaces studied. XPS analysis of the carbon surfaces after TPD shows that no SO_2 remains, therefore, the desorption peak areas can be used as a relative measure of the amounts of SO_2 adsorbed by the different carbon surfaces. Differences in the slopes of the lines reflect differences in both SO_2 sticking coefficient and adsorption site density. The a-C surface adsorbs the most SO_2, likely due to a high density of high energy edge defect sites. As described earlier, post-treatment of a-C by exposure to O_2 blocks a fraction of the a-C edge sites to form a-CO_x; in Fig. 5, this effect is reflected as a smaller slope for a-CO_x than for a-C.

The coverage-exposure plots for HOPG, a-CN_x, and a-CH_x also display lower slopes than a-C. These surfaces do not possess the high energy edge defects; their interactions with SO_2 occur via the weaker π-bond and could be characterized by lower sticking coefficients. There are subtle, but potentially important, differences among this trio: HOPG adsorbs the most SO_2 followed by a-CN_x and a-CH_x. This is the same order as their E_{des}, suggesting that stronger interaction between condensed SO_2 islands and the surface may promote formation of more or larger islands.

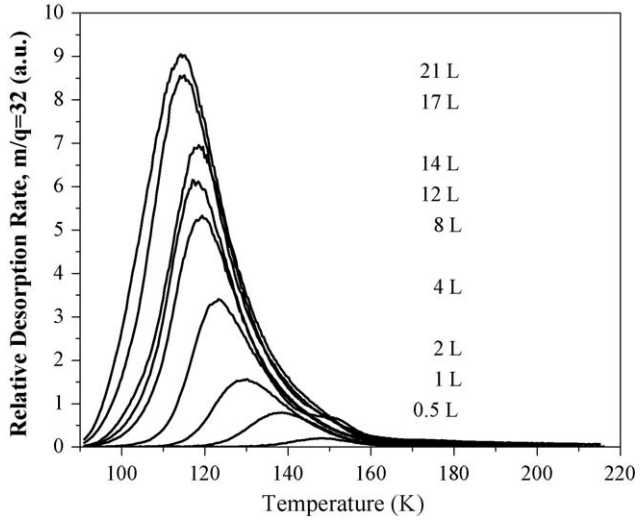

Fig. 9. Temperature programmed desorption of H_2S from a-C for different exposures. Exposures were performed at ~90 K; the heating rate was 1 K/s. Peak shapes suggest first-order desorption from an energetically heterogeneous surface.

3.2. Interactions of H_2S with the carbon surfaces

Exposures as high as 20 L at 92–110 K did not result in the adsorption of H_2S onto the HOPG, a-CN_x or a-CH_x surfaces. Note that these are the three surfaces on which SO_2 adsorbed through self-interaction to form islands bound via weak van der Waals interactions with π-electrons in the aromatic rings of the carbon surface. H_2S has a significantly lower value of ΔH_{sub} than SO_2 (23.01 vs. 32.32 kJ/mol) [31], reflecting a lower degree of self-interaction which may prevent condensation and island formation on these surfaces.

Thermal desorption spectra of H_2S from the a-C and a-CO_x surfaces, after exposures in the range 0.5–21 L are shown in Figs. 9 and 10, respectively. On both surfaces, H_2S desorption is first-order, with the peak desorption temperature varying from 150 (low coverage) to 115 K (high coverage). This trend is similar to that observed for SO_2 on the a-C and a-CO_x surfaces, suggesting that H_2S also binds at edge defect sites. Using the first-order Redhead analysis with a pre-exponential factor of $\nu = 10^{13}$ s^{-1}, the values of E_{des} for desorption of H_2S from both a-C and a-CO_x were estimated. For both surfaces, the value of E_{des} varied from 39 ± 1 (low coverage) to 30 ± 1 kJ/mol (high coverage). These values are larger than H_2S' heat of sublimation, ΔH_{sub} = 23.01 kJ/mol [31]; they fall between the values of E_{des} = 20.6 kJ/mol reported by Doleva et al. for H_2S on carbon black [34] and the range of values reported by Bagreev et al. for a number of commercial activated carbons (E_{des} = 39 – 47 kJ/mol) [17]. According to Bagreev et al., the larger values of E_{des} on commercial activated carbons results from their microporosity. Effects such as capillary condensation contribute to a higher effective activation barrier to desorption.

As was the case for SO_2, post treatment of a-C to form a-CO_x does not affect the kinetics of H_2S desorption, but does reduce its capacity for H_2S adsorption. Therefore the oxygen species appears to inhibit adsorption via the site blocking mechanism described for SO_2.

4. Conclusion

We have applied the methods of ultra-high vacuum surface science to characterize adsorption and desorption of SO_2 and H_2S

for a series of model carbon surfaces. We have shown that both microstructure and chemical composition of carbonaceous materials contribute to their interactions with SO_2 and H_2S. SO_2 and H_2S interact with the carbon surfaces via two primary mechanisms. First, both sulfur-compounds can adsorb at unsaturated defect sites at the periphery of aromatic sheets within the carbon structure. These "edge defects" exist in a variety of configurations leading to an energetically heterogeneous surface that displays a distribution of desorption energies, E_{des}. This type of site is responsible for the relatively strong adsorption of SO_2 and H_2S onto a-C and a-CO_x; desorption from these surfaces proceeds via first-order kinetics. Second, SO_2 can condense as islands that are weakly bound to the surface, probably via van der Waals interaction with the π-electron systems in the aromatic carbon structure. Desorption from the island edges occurs via a zero-order process. This pattern is characteristic of adsorption of SO_2 onto HOPG, a-CN_x, and a-CH_x. Although H_2S was not observed to interact with these surfaces, adsorption must occur at temperatures lower than those accessible in this work and may also exhibit zero-order desorption kinetics.

Since adsorption and desorption are key primary steps in capture and release of sulfur-compounds by industrially-relevant activated carbon sorbents, our results can provide guidance for development of next-generation carbons. Clearly, maintaining a high density of surface defects, such as those present in a-C, is important for development of sorbents with high affinity and capacity for sulfurous-gases. However, post-oxidation of a-C appears to titrate surface defects, thereby reducing the density of adsorption sites. Incorporation of H or N into the developing carbon structure minimizes formation of surface defects and reduces the strength of the interaction between condensed SO_2 islands and the surface.

Acknowledgements

The authors thank Radisav Vidic and Jason Monnell at the University of Pittsburgh for helpful discussions.

This technical effort was performed in support of the National Energy Technology Laboratory under the RDS contracts DE-AC26-04NT41817.606.01.05 and DE-AC26-04NT41817.630.01.10.

References

[1] S. Bashkova, et al. Carbon 45 (2007) 1354–1363.
[2] I. Mochida, et al. Journal of the Japan Petroleum Institute 47 (2004) 145–163.
[3] J. Nhut, et al. Catalysis Today 91–92 (2004) 91–97.
[4] A. Primavera, et al. Applied Catalysis A 173 (1998) 185–192.
[5] A.L. Kohl, R.B. Nielson (Eds.), Gas Purification, 5th ed., Gulf Publishing, Houston, TX, 1997.
[6] G.J. Stiegel, M. Ramezan, International Journal of Coal Geology 65 (2006) 173–190.
[7] F. Adib, A. Bagreev, T.J. Bandosz, Langmuir 16 (2000) 1980–1986.
[8] T.J. Bandosz, Journal of Colloid and Interface Science 246 (2002) 1–20.
[9] R.M.A. Roque-Malherbe, Adsorption Diffusion in Nanoporous Materials, CRC Press, Boca Raton, 2007.
[10] L. Meljac, et al. Journal of Colloid and Interface Science 274 (2004) 133–141.
[11] W. Feng, et al. Environmental Science & Technology 239 (2005) 9744–9749.
[12] F. Rodriguez-Reinoso, Carbon 36 (1998) 159–175.
[13] A.C. Ferrari, J. Robertson, Physical Review B 61 (2000) 14095–14107.
[14] J. Robertson, Materials Science and Engineering R 37 (2002) 129–281.
[15] I. Mochida, S.H. Yoon, W. Qiao, Journal of the Brazilian Chemical Society 17 (2006) 1059–1073.
[16] A. Bagreev, H. Rahman, T.J. Bandosz, Environmental Science & Technology 34 (2000) 4587–4592.
[17] A. Bagreev, H. Rahman, T.J. Bandosz, Carbon 39 (2001) 1319–1326.
[18] A. Begreev, F. Adib, T.J. Bandosz, Carbon 39 (2001) 1897–1905.
[19] M.P. Cal, B.W. Strickler, A.A. Lizzio, Carbon 38 (2000) 1757–1765.
[20] S.V. Mikhalovsky, Y.P. Zaitsev, Carbon 35 (1997) 1367–1374.
[21] M. Steijns, P. Mars, Journal of Catalysis 35 (1974) 11–17.
[22] M. Steijns, P. Mars, Journal of Colloid and Interface Science 57 (1976) 175–180.
[23] Y. Yun, E. Broitman, A.J. Gellman, Langmuir 23 (2007) 1953–1958.
[24] E. Broitman, J. Neidhart, L. Hultman, in: C. Donnet, A. Erdemir (Eds.), Tribology of Diamond-like Carbon Films: Fundamentals and Applications, Springer, 2007, pp. 620–654.
[25] Y. Yun, et al. Langmuir 23 (2007) 5485–5490.
[26] N. Hellgren, et al. Journal of Vacuum Science Technology A 18 (2000) 2349–2358.
[27] A.M. de Jong, J.W. Niemantsverdriet, Surface Science 233 (1990) 355–365.
[28] E. Habenschaden, J. Kuppers, Surface Science 138 (1984) L147–L150.
[29] J.A. Rodriguez, et al. Chemical Physics Letters 378 (2003) 526–532.
[30] T.W. Schlereth, et al. Journal of Physical Chemistry 109 (2005) 20895–20905, T.E..
[31] R.H. Perry, D.W. Green (Eds.), Perry's Chemical Engineer's Handbook, 7th ed., McGraw-Hill, New York, 1997.
[32] F. Rodriguez-Reinoso, M. Molina-Sabio, M.A. Munecas, Journal of Physical Chemistry 96 (1992) 2707–2713.
[33] P.A. Redhead, Vacuum 12 (1962) 203–211.
[34] I.A. Doleva, A.V. Kiselev, Y.I. Yashin, Zhurnal Fizicheskoi Khimii 48 (1974).